ACS APPLIED ENERGY MATERIALS

www.acsaem.org

Article

From Additive to Cosolvent: How Fluoroethylene Carbonate Concentrations Influence Solid−Electrolyte Interphase Properties and Electrochemical Performance of Si/Gr Anodes

Lydia Gehrlein, Christian Njel, Fabian Jeschull, and Julia Maibach*

Cite This: *ACS Appl. Energy Mater.* 2022, 5, 10710−10720

Read Online

ACCESS | Metrics & More | Article Recommendations | Supporting Information

ABSTRACT: Silicon-containing anodes perform best when the solid−electrolyte interphase (SEI) accommodates the high volume changes of silicon particles, as this reduces side reactions and extends the cell lifetime. With this work, we investigate the influence of different fluoroethylene carbonate (FEC) electrolyte concentrations on the SEI composition and thickness and correlate these SEI properties to the electrochemical performance. Three electrolytes (i.e., 2FEC:98LP30, 20FEC:80DMC, and 50FEC:50DMC) are cycled with 9% Si/Gr anodes, and their SEIs are characterized postmortem using photoelectron spectroscopy (XPS). We propose a fitting model for the XPS results in which FEC decomposition yields −C−O, DO (1,3-dioxolan-2-one), $-CO_2Li$, Li_2CO_3, and LiF. −C−O, DO, and $-CO_2Li$ are most probably incorporated in a cross-linked polymeric network. Due to its distinct chemical environments, detecting DO can be unambiguously linked to the presence of FEC decomposition products in the SEI. The presence of DO-type species in the C 1s spectra is correlated to the electrochemical performance: A higher retention in silicon activity was observed for the 20 and 50 vol % FEC-containing electrolytes, where FEC decomposition products (i.e., DO) were present even after 100 cycles. By contrast, when cycling in the 2FEC:98LP30 electrolyte, the silicon activity cannot be retained, and FEC decomposition products are barely detected after 100 cycles. We suggest that the presence of the −C−O-, DO-, and $-CO_2Li$-containing polymeric network positively influences the SEI during silicon volume changes. Additionally, we show that the interaction of FEC and $LiPF_6$ plays an important role in the formation of SiO_xF_y species.

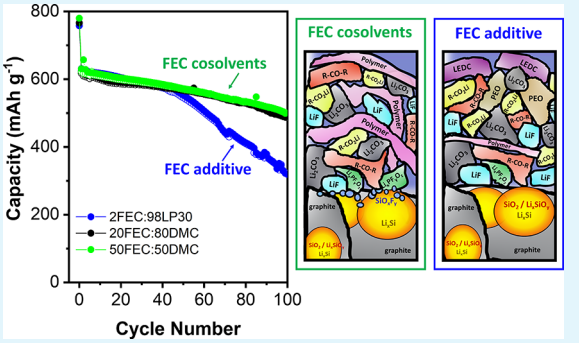

KEYWORDS: *silicon anodes, silicon-graphite anodes, FEC, solid−electrolyte interphase (SEI), EC-free electrolytes, photoelectron spectroscopy (XPS), lithium-ion batteries*

1. INTRODUCTION

In lithium-ion batteries, the stability of the solid−electrolyte interphase (SEI) is essential to a long cycle life. During lithiation, the electrolyte is repeatedly exposed to potentials outside its stability window (<1.3−0.8 V), resulting in its decomposition and deposition of solid products on the anode surface building the SEI.[1] Especially in the first cycle, while the electrode surface is still bare, electrolyte decomposition occurs to a high degree. Many of these decomposition products are irreversibly formed and are depleting the lithium reservoir, which causes large capacity losses and low Coulombic efficiencies. However, once formed, the SEI ideally acts as a protective barrier, minimizing electrolyte reduction.[2] Whether the SEI layer is operating as a protective barrier is mainly dependent on the nature of the formed electrolyte decomposition products as well as the electrode material. This is especially the case for materials such as silicon with high volume changes during lithiation and delithiation processes.

While silicon delivers high theoretical capacities (i.e., Q_{th} = 3579 mA h g^{-1}), it displays high volume changes (~300%) upon lithiation and delithiation.[3] As a result, silicon particles may pulverize, and the electrode material can delaminate from the current collector. Additionally, these volume changes cause high mechanical stress on the SEI, leading to cracks and re-exposure of silicon particles to the electrolyte.[4−8] This leads to continuous SEI formation, thus depleting the lithium reservoir and electronically isolating silicon particles. Ultimately, these effects result in capacity fading and the cell's end of life. Blending silicon with graphite can mitigate these effects.[9,10] Graphite's positive effects are (1) reduction of the stress on the electrode coating by providing a porous structure that accommodates the silicon volume change,[11] (2) mitigation of

Received: May 12, 2022
Accepted: July 21, 2022
Published: August 24, 2022

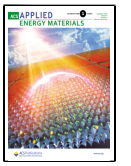

electronic contact losses,[10,12,13] and (3) a decrease of SEI formation.[14] However, the overall electrochemical performance still heavily depends on the electrolyte used. Additive-free carbonate-based electrolytes such as LP30 (1 mol of $LiPF_6$ in 1:1 ethylene carbonate:dimethyl carbonate) have been shown to form very unstable SEIs on silicon-containing anodes. For this type of electrolyte, both $LiPF_6$ salt decomposition products such as LiF, Li_xPF_y, and $Li_xPF_yO_z$ and solvent decomposition products like lithium carbonate (Li_2CO_3), lithium alkoxy compounds (LiOR), lithium ethylene dicarbonate (LEDC), and polyethylene oxide (PEO) are observed.[15,16] In particular, LEDC and PEO are suspected of not being able to accommodate the volume changes of the silicon particles: solid-state NMR (ss-NMR) analyses of cycled electrolyte solution detected a high concentration of short-chain lithium alkyl carbonates and PEO-type oligomers, suggesting high solubility of these decomposition products.[17]

Adding electrolyte additives such as fluoroethylene carbonate (FEC) greatly enhances the electrochemical performance of Si/Gr anodes. Several FEC decomposition mechanisms and associated stabilizing effects have been proposed to date. Many of them point to the formation of a cross-linked polymer that can adapt to changes in the electrode volume. Direct reduction of FEC with Li-naphthalene yielded the formation of cross-linked polymerized vinylene carbonate (poly(VC)) units that were detected by ss-NMR, XPS, and FTIR.[18] An ss-NMR study of electrochemically generated FEC decomposition products found cross-linked polymers with both poly(VC) and PEO units.[19] Another study from the same authors found no short-chain PEO and LEDC in the electrolyte when FEC was used.[17] This strongly suggests that the cross-linked nature of these polymers stabilizes the SEI during the electrode volume changes and effectively suppresses EC decomposition. However, FEC is continuously consumed upon cycling as has been shown in online electrochemical mass spectrometry (OEMS).[20] The stabilizing effect of FEC is retained only as long as the additive is present in the cell. The complete depletion of FEC is followed by EC reduction and an increase of the cell polarization leading to a rapid capacity drop. Also, the consumption of FEC seems to take place during both lithiation and delithiation processes.[21] Other known FEC decomposition products include LiF, Li_2CO_3, and other carbonate-containing species, carboxylic and carbonyl environments, and acetal-based compounds. Regarding C−F and Si−F environments, the literature is divided. While XPS measurements indicate C−F and Si−F species,[22−25] they could not be detected via ss-NMR.[18,19] Along with its influence on SEI properties, FEC appears to affect the interaction between the SEI and the electrode.[26] Its presence seems to promote the formation of organosiloxane (i.e., −Si−C−) species and thereby influences the adhesion of the organic SEI to silicon surfaces.[19] FEC is not only used as an electrolyte additive but also as an electrolyte solvent to replace ethylene carbonate (EC).[21,27,28] This approach is especially followed for electrolytes also used at high voltages. Substituting EC by fluorinated compounds such as FEC, F2EC, and fluorinated ether (FEPE) has been shown to improve the cycling behavior of high-voltage cathodes.[29−31]

In this study, we investigate three electrolyte formulations with FEC concentrations ranging from additive (i.e., 2 vol %) to cosolvent (i.e., 20 and 50 vol %), resulting in the following electrolyte mixtures: 2FEC:98LP30, 20FEC:80DMC, and 50FEC:50DMC. We analyze how the FEC content influences the SEI composition, thickness, and electrode morphology. SEI properties are studied by X-ray photoelectron spectroscopy (XPS), and scanning electron microscopy (SEM) is used to study the electrode morphology. To achieve conclusive data evaluation, we present a general fitting model for FEC decomposition products. Finally, we demonstrate how the SEI, which depends on the FEC content in the electrolyte, influences the electrochemical performance of Si/Gr electrodes.

2. EXPERIMENTAL SECTION

2.1. Electrolyte Preparation. A battery-grade LP30 electrolyte (i.e., 1 M lithium hexafluorophosphate in a 1:1 mixture of ethylene carbonate:dimethyl carbonate), a hexafluorophosphate ($LiPF_6$) salt, a dimethyl carbonate (DMC) solvent, and a fluoroethylene carbonate (FEC) electrolyte additive were purchased from Merck and used as received. The $LiPF_6$ salt was dried under vacuum at 110 °C for 12 h. The FEC additive electrolyte was prepared by mixing 98 vol % LP30 with 2 vol % FEC. For both FEC cosolvent formulations, the respective volume fractions of DMC and FEC were mixed with 1 M dried $LiPF_6$ salt. The water content of all three electrolytes was measured by Karl Fischer titration to be <10 ppm. All electrolytes were prepared in a glovebox.

2.2. Electrode Preparation. Electrodes were prepared using a slurry of 81 wt % graphite (SFG6L, Imerys Graphite & Carbon, Switzerland), 9 wt % silicon nanopowder (Nanostructured & Amorphous Materials, Inc., 50−100 nm, purity of >99%), 5 wt % carbon nanofibers (Showa Denko), and 5 wt % lithium-polyacrylic acid binder solution. The binder solution was obtained by diluting a ready-made 45 wt % polyacrylic acid in a water solution (Sigma Aldrich) and subsequently adding lithium hydroxide (LiOH, Sigma Aldrich) until a pH of 6.5 was reached. The slurries were prepared in a two-step process. Premixing was done in a planetary mixer (Thinky ARV-310P). Hereby, silicon nanopowder (9 wt %) was mixed with carbon nanofibers (5 wt %) and graphite (81 wt %) in a water:ethanol mixture of 1:1.2. Subsequently, the mixture was dried and gradually transferred into a glass vial containing the binder solution. To break particle agglomeration, mixing was performed via ultrasonic dispersion with an ultrasonic homogenizer (Kinematica, Polytron PT 2500). The obtained slurry was coated on copper foil with a doctor blade (the wet thickness was set to 150 μm) and later dried at room temperature overnight. Individual electrodes were cut into discs of 12 mm diameter and dried under vacuum at 120 °C for 12 h. The resulting electrodes had a silicon-graphite mass loading of around 2.8−3.1 mg/cm^2.

2.3. Half-Cell Assembly and Cycling. The half-cells were assembled in an Ar-filled glovebox using a CR2025-type coin cell half-cell setup. The cells consisted of the Si/Gr working electrode, a microporous polypropylene separator (Celgard 2325), a glass fiber separator (VWR), and Li foil (thickness of 0.25 mm, purity of 99.9%, PI-KEM) as the counter electrode. The Celgard 2325 separator was applied directly on the electrode surface to protect the surface from glass fiber contaminations. The respective electrolyte solution (150 μL) was used. Galvanostatic cycling with potential limitation (GCPL) was performed with a multichannel potentiostat (VMP3 & BCS, Bio-Logic) at 25 °C in a climate chamber (Binder). After one formation cycle at C/20 (Q_{th} = 623 mA h g^{-1}), all cells were cycled at a lithiation rate of C/10 and a delithiation rate of C/3 between 1.5 and 0.01 V. All potentials are given in reference to Li/Li$^+$. After every lithiation step, a constant-current−constant-voltage (CCCV) step was applied at C/5 for 30 min.

2.4. Postmortem Analysis (XPS and SEM). All electrode samples were washed by a 1 min submersion in 1 mL of dimethyl carbonate (DMC) to remove excess electrolyte after cycling. After washing, all electrodes were dried and mounted on a sample holder using conductive copper tape. Sample preparation was carried out in an argon-filled glovebox (H_2O and O_2 < 1 ppm). Transfer to the XP spectrometer or the SEM was done via a transfer module under inert

https://doi.org/10.1021/acsaem.2c01454
ACS Appl. Energy Mater. 2022, 5, 10710−10720

gas conditions. To ensure SEI stability in lithiated and delithiated states, the lithiation and delithiation endpoint potentials were held for 1 h after the electrochemical cycling.

2.4.1. X-ray Photoelectron Spectroscopy (XPS). XPS measurements were carried out with a K-alpha spectrometer from Thermo Fisher Scientific applying a microfocused, monochromated Al Kα X-ray source with a 400 μm spot size. A pass energy of 50 eV was used. Data acquisition and handling were done via Thermo Avantage software according to Parry *et al.*[32] Spectra were fitted with one or more Voigt profiles, and Scofield sensitivity factors were applied for quantification. All spectra were referenced in binding energy to the hydrocarbon C 1s peak at 285 eV. For clarity of presentation, all spectra were normalized in intensity to the maximum intensity (i.e., the highest peak and background are normalized in intensity to [1,0]).

2.4.2. Scanning Electron Microscopy (SEM). Scanning electron microscopy (SEM) measurements were conducted using a thermal field emission scanning electron microscope (FESEM, Carl Zeiss SMT AG) equipped with energy-dispersive spectroscopy (EDS, Quantax 400 SDD, Bruker) at an acceleration voltage of 7 kV.

3. RESULTS AND DISCUSSION

3.1. Electrochemistry. Galvanostatic cycling results of 9% Si/Gr half-cells cycled in the respective electrolytes 2FEC:98LP30 (blue), 20FEC:80DMC (black), and 50FEC:50DMC (green) are shown in Figure 1.

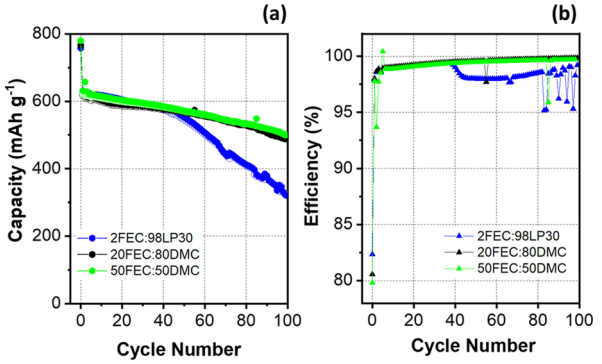

Figure 1. (a) Cycling stabilities (filled circles for lithiation and hollow circles for delithiation) and (b) Coulombic efficiencies of Si/Gr electrodes cycled in 2FEC:98LP30 (blue), 20FEC:80DMC (black), and 50FEC:50DMC (green) electrolytes.

All three cells display similar initial lithiation capacities of around 765 mA h g^{-1}, independent of the electrolyte. This value is much higher than the expected theoretical capacity of 623 mA h g^{-1} due to extensive SEI formation during the first lithiation. Therefore, the resulting Coulombic efficiencies amount to only 80−83%. After the first delithiation, a capacity of around 620 mA h g^{-1} is reached, which is close to the theoretical one. Upon cycling, the cell containing 2FEC:98LP30 exhibits the fastest capacity fade. After around 40 cycles, a linear decrease can be observed, which results in a capacity loss of 309 mA h g^{-1} after 100 cycles and a retention of only 51%, when compared to the second cycle capacity. The loss in electrochemical activity at around 40 cycles can also be observed in the Coulombic efficiency plot, where efficiencies decrease to 98%. By contrast, when using the FEC cosolvent electrolytes, a more stable cycling behavior is achieved. Electrodes cycled in 20FEC:80DMC and 50FEC:50DMC exhibit higher lithiation capacity retentions after 100 cycles when compared to the second cycle, amounting to 78 and 79%, respectively. Usually, capacity retentions of 75−80% declare the end of life of an LIB. However, the purpose of this study is to determine the effect of varying FEC concentrations on cycling stability rather than to optimize the battery cycle life. The drop in capacity can be attributed to the loss in silicon activity, as can be seen in the dQ/dE inset of Figure S1a. A positive effect of FEC on the electrochemical performance and more specifically on the retention of silicon activity has been demonstrated in several studies.[7,20,22,33−38] Also, it has been shown by Jung *et al.* that FEC is consumed in every cycle, and when depleted, the cell performance drops dramatically.[20] Hereby, the consumption of FEC is dependent on the relation of FEC concentration and the amount of active material in the electrode (i.e., $\mu mol_{FEC}/mg_{electrode}$). In our case, all electrodes exhibited the same amount of silicon and a similar mass loading of around 2.8−3.1 mg cm^{-2}. FEC consumption on the lithium metal counter electrode has been observed in the literature;[20] however, we can assume that these effects are very similar between our cells, as a similar cell setup with lithium counter electrodes was used. Therefore, the drop in capacity for the electrode cycled in the FEC additive electrolyte 2FEC:98LP30 shows the fastest capacity drop because FEC seems to be depleted earlier. With FEC as a cosolvent, a sufficient amount of FEC is still present in the electrolyte. In the following, we investigated how the FEC concentration in the electrolyte influences the SEI composition, thickness, and the electrode morphology.

3.2. SEI Analysis. *3.2.1. SEI Thickness on Graphite Particles.* In this work, the SEI thickness is calculated by considering an average photoelectron inelastic mean free path, see Supporting Information page S3 for details. The calculation was conducted for Si/Gr anodes cycled to 0.8 and 0.01 V during the first lithiation as well as to 1.5 V after the 1st, 10th, and 100th delithiation. Obtained thicknesses are displayed in Figure 2. At 0.8 V, the SEI thickness is below 5 nm for all

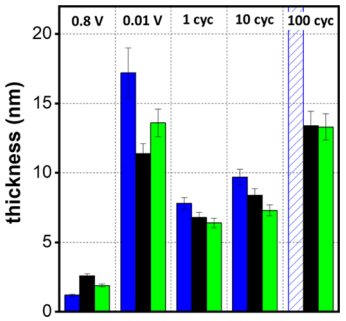

Figure 2. SEI thickness on graphite in Si/Gr electrodes cycled in 2FEC:98LP30 (blue), 20FEC:80DMC (black), and 50FEC:50DMC electrolytes (green) at 0.8 and 0.01 V during the first lithiation and at 1.5 V after the 1st, 10th, and 100th cycle. The error bars consider the error of the fitting procedure and the IMPF average. The hatched column for 2FEC:98LP30 indicates that the SEI is thicker than the XPS information depth.

electrolyte formulations. Because carbonate-based solvents are known to decompose at around 1.2−0.9 V vs Li/Li$^+$, the SEI is still thin at this early stage.[39] In the fully lithiated state at 0.01 V, the thickness increases considerably for all three FEC contents. After the first delithiation at 1.5 V, a drop in SEI thickness is seen for all three electrolytes. This phenomenon of changes in SEI thickness from lithiated to delithiated states is known as SEI breathing and is a commonly observed process for silicon-containing electrodes.[40,41] After 10 cycles, the thickness increases for each electrolyte. This increase is even

https://doi.org/10.1021/acsaem.2c01454
ACS Appl. Energy Mater. 2022, 5, 10710−10720

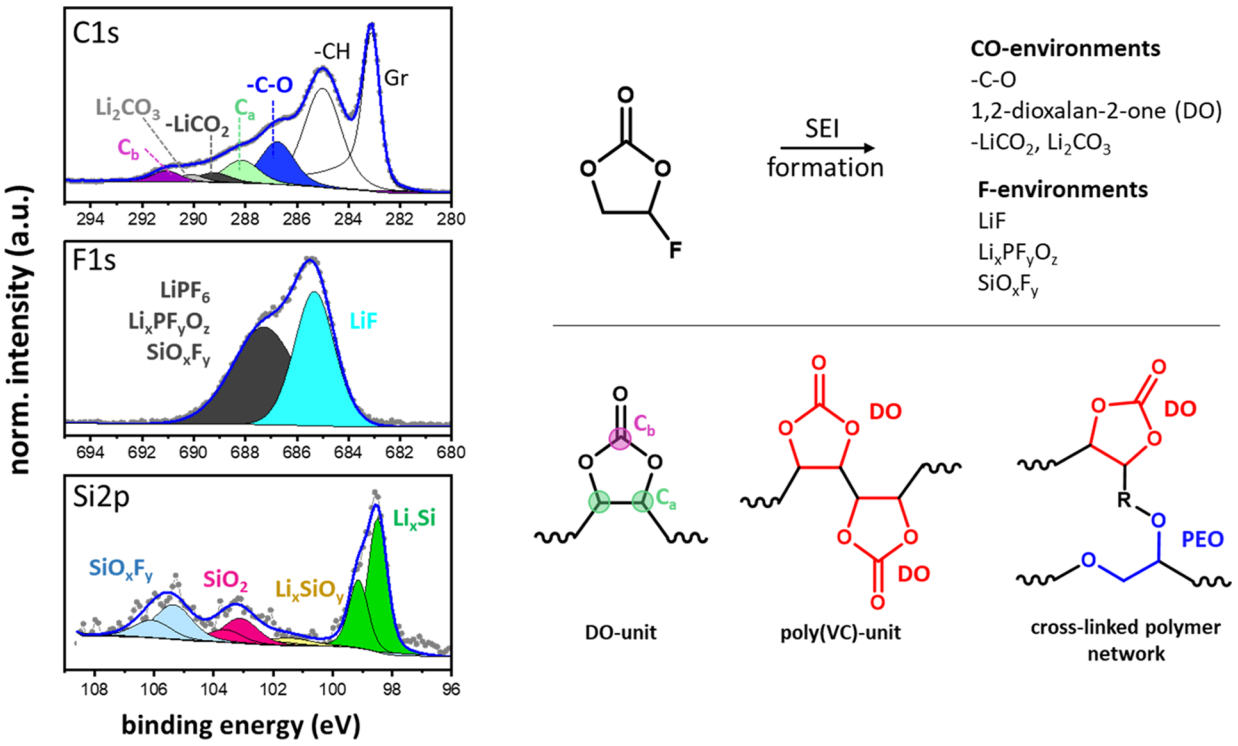

Figure 3. C 1s, F 1s, and Si 2p photoelectron spectra of an electrode after the first lithiation cycled in 1 M $LiPF_6$ in an FEC electrolyte. Decomposition products of FEC based on refs 17, 19, and 25.

stronger after 100 cycles, indicating the formation of a thick SEI layer on the graphite particles. In the case of 2FEC:98LP30, no graphite intensity was detected, indicating an SEI thickness above the information depth of XPS, and the column in Figure 2 is therefore hatched. In contrast, when cycled in 20FEC:80DMC and 50FEC:50DMC, the SEI thickness is still below that critical threshold with values amounting to approximatively 13 nm. Overall, a correlation in SEI thickness and FEC electrolyte concentration can be observed for the cycling stages at 0.01 V, 1, 10, and 100 cycles. The less FEC is present in the electrolyte, the thicker the SEI: 2FEC:98LP30 > 20FEC:80DMC > 50FEC:50DMC.

3.2.2. XPS Fitting Model of FEC Decomposition. For the purpose of studying the decomposition products of FEC, we analyzed the SEI formed by a pure FEC electrolyte (i.e., 1 mol of $LiPF_6$ in 100% FEC) on Si/Gr electrodes after cycling to 0.01 V. The resulting C 1s, F 1s, and Si 2p spectra are displayed in Figure 3. O 1s and P 2p spectra are shown in the Supporting Information (Figure S2a). Alongside hydrocarbon (285 eV) and graphite (283.4 eV), the following carbon−oxygen environments can be identified in the C 1s spectrum: −C−O (286.8 eV), C_a (287.9 eV), $-CO_2Li$ (289.2 eV), Li_2CO_3 (290.2 eV), and C_b (291.1 eV). C_a and C_b represent the two carbon environments in 1,3-dioxolan-2-one (DO), see the molecular structure in Figure 3. The fitting of this species was done based on previous data for this environment.[42] We further fixed the FWHM and the area ratio between C_a and C_b to 2:1 during fitting. The detection of DO in our XPS measurement can be an indication for FEC defluorination, yielding LiF and VC. VC can subsequently polymerize and form poly(VC). To check whether VC forms a similar SEI, we analyzed the decomposition products of an electrode cycled in pure VC. The C 1s spectrum in Figure S2b displays two peaks corresponding to C_a and C_b in poly(VC).[42] Only little amounts of −C−O and $-CO_2$ and no Li_2CO_3 are detected. In contrast, FEC leads to an SEI with high −C−O, C_a/C_b, and $-CO_2Li$ contents. This demonstrates that the SEIs formed by FEC and VC are very different. As proposed in the literature, it is very likely for DO or poly(VC), −C−O, and $-CO_2Li$ units to form a heterogeneous cross-linked polymer network.[17−19,43,44] For example, Jin *et al.* proposed a polymer consisting of cross-linked DO and PEO units.[19] The −C−O groups detected in our XPS analysis could correspond to PEO species. It is important to note that XPS cannot differentiate between poly(VC) and DO units as they display identical chemical environments at the same binding energies. It is also not possible to get information on the exact molecular structure of the polymer network with XPS due to the highly inhomogeneous nature of the SEI. A decomposition mechanism for FEC is proposed in Figure S3. The F 1s spectrum of Figure 3 shows a peak at 685.3 eV corresponding to LiF and a broad peak at 687.7 eV that is most likely a mixture of $LiPF_6$ salt residues, $Li_xPF_yO_z$ salt decomposition products, and silicon oxyfluorides SiO_xF_y.[45] Both F−P and F−Si environments can be found in the corresponding P 2p (Figure S2a in the SI) and Si 2p spectra (Figure 3), respectively. LiF is a result of $LiPF_6$ and FEC decomposition. Different silicon environments emerge in the Si 2p spectrum, namely, Li_xSi (98.2 eV), Li_xSiO_y (101 eV), SiO_2 (103 eV), and SiO_xF_y (105.3 eV).[23,24] To ensure consistent data evaluation, this fitting is used in all the following XPS analyses. Detailed information about the used fitting parameters can be found in Table S1.

3.2.3. SEI Composition. Figure 4 displays C 1s photoelectron spectra of Si/Gr electrodes cycled in 2FEC:98LP30, 20FEC:80DMC, and 50FEC:50DMC. Spectra for the following cycling states are shown: 0.8 and 0.01 V during the first lithiation as well as the 1st, 10th, and 100th cycle in

https://doi.org/10.1021/acsaem.2c01454
ACS Appl. Energy Mater. 2022, 5, 10710−10720

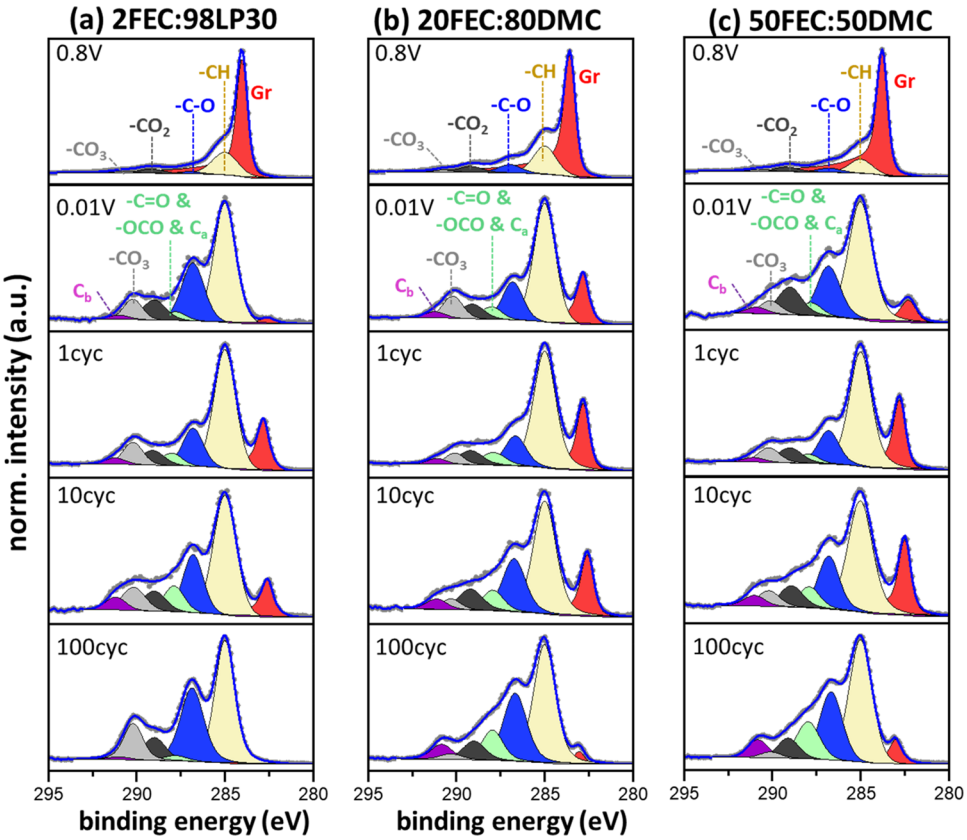

Figure 4. C 1s photoelectron spectra of electrodes cycled in (a) 2FEC:98LP30, (b) 20FEC:80DMC, and (c) 50FEC:50DMC electrolytes at 0.8 and 0.01 V during the first lithiation and at 1.5 V after the 1st, 10th, and 100th cycle.

delithiated states at 1.5 V. Derived atomic percentages of detected C 1s species are shown in Figure 5. Also displayed in Figure 5 are the atomic percentages of fluorine-containing decomposition products. F 1s, O 1s, and P 2p spectra can be found in the Supporting Information, see Figures S4–S6. An overview of all detected species with their atomic percentages is shown in Tables S2–S4 (SI). Assignment of different surface species has been done according to the fitting model previously described.

At 0.8 V, five peaks are observed for each electrolyte in the C 1s spectra of Figure 4: graphite (~284.2 eV), hydrocarbons (285 eV), −C−O groups (~286.7 eV), $-CO_2Li$ species (289.2 eV), and $-CO_3Li$ species (~290.5 eV). Hydrocarbons can originate from surface contamination such as adventitious carbon as well as from −CH-containing SEI species. All −CO-containing compounds originate from starting electrolyte decomposition. A further voltage decrease to 0.01 V leads to thickening of the SEI, as can be seen by a drop in graphite intensity. As previously seen, the SEI thickness depends on the amount of FEC in the electrolyte and follows the trend 2FEC > 20FEC > 50FEC. A shift to lower binding energies of the graphite peak (i.e., to 282.5 eV) can be explained by the formation of an electrical potential gradient at the buried interface between the SEI and the electrode surface.[46,47] Additionally, two peaks emerge that can be ascribed to the two carbon environments in DO as has been previously discussed, namely, C_a (287.9 eV) and C_b (291.0 eV). The intensity ratio of C_a and C_b is close to 1:2, suggesting that the peaks mainly consist of DO units. Compared to the C 1s of the electrode cycled in pure FEC (see Figure 3), the same carbon species are detected. While −CH, −C−O, $-CO_2Li$, and $-CO_3Li$ were observed with pure FEC electrolytes, these species typically also emerge in SEIs formed by DMC- and EC-containing electrolytes, see Figure S7. Only C_a and C_b emerge in the presence of FEC. In the following discussion, these peaks are

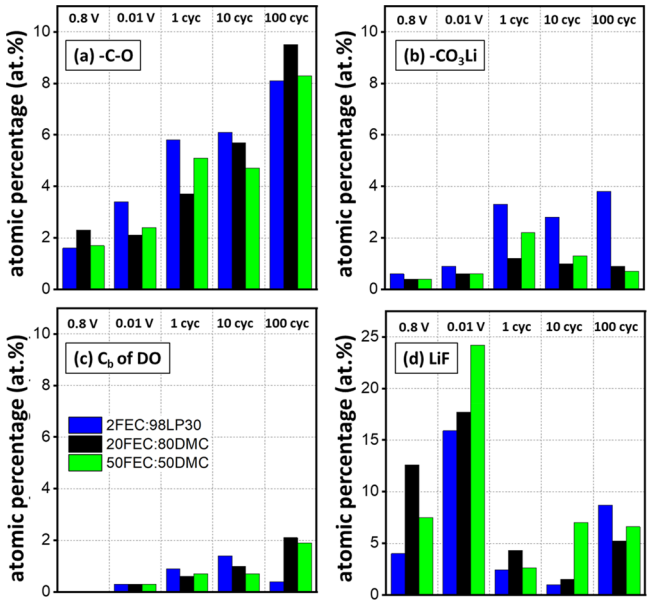

Figure 5. Atomic percentages of (a) −C−O, (b) $-CO_3$, (c) C_b in poly(VC), and (d) LiF. Displayed are the percentages at 0.01 V during the first lithiation and at 1.5 V after the 1st, 10th, and 100th cycle for the respective electrolyte, i.e., 2FEC:98LP30, 20FEC:80DMC, and 50FEC:50DMC.

https://doi.org/10.1021/acsaem.2c01454
ACS Appl. Energy Mater. 2022, 5, 10710−10720

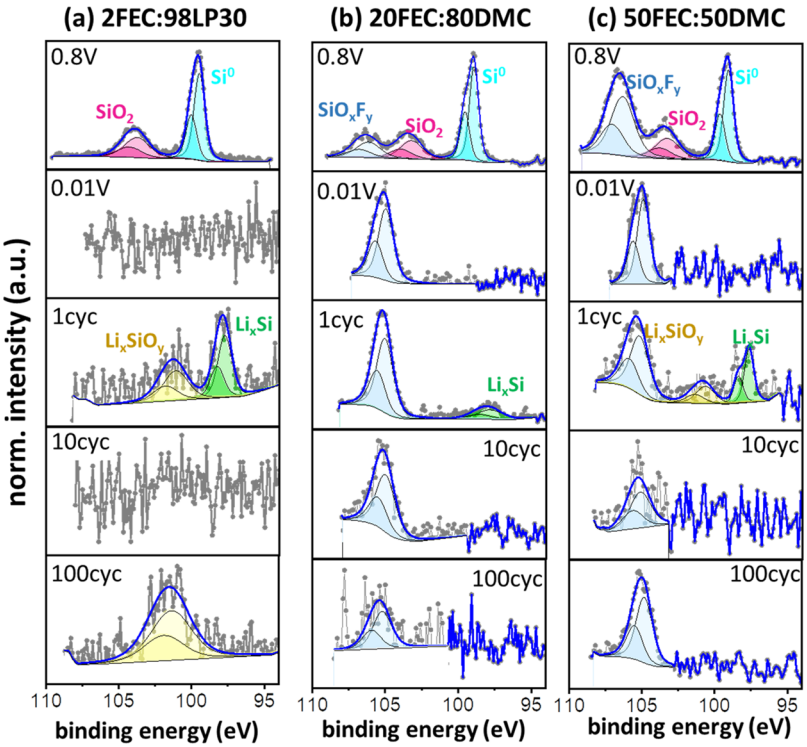

Figure 6. Si 2p photoelectron spectra of 9% Si/Gr half-cells cycled in (a) 2FEC:98LP30, (b) 20FEC:80DMC, and (c) 50FEC:50DMC.

therefore used as an unambiguous indicator for the presence of FEC decomposition products in the SEI (the emergence of LiF also occurs for $LiPF_6$ and FEC, making it difficult to differentiate from which electrolyte component LiF is originating). After the first delithiation to 1.5 V, the graphite intensity increases for all three cases, indicating a thinner SEI. The SEI thinning results from the dissolution or detachment of certain species, such as LiF, which drops by 20 at. %, see Figure 5. A decrease in the relative peak area is observed for −C−O and $-CO_2Li$ compounds, see Figure S7, while carbonate and DO species only change to a negligible extent. After 10 cycles, a decrease in atomic percentages and relative peak areas of carbonate species is observed for all three electrolytes, see Figure 5 and Figure S7. Electrodes cycled in 2FEC:98LP30 and 20FEC:80DMC display an increase in −C−O and DO abundance, while the detected LiF amount decreases. By contrast, the electrodes cycled in 50FEC:50DMC show no changes for −C−O and DO species but an increase in LiF. After 100 cycles, a large decrease of C_a and C_b is observed with 2FEC:98LP30, while −C−O and $-CO_3$ species increase in intensity and abundance, see Figures 4 and 5. In fact, the spectrum now looks very similar to a spectrum from an electrode cycled in a pure LP30 electrolyte, see Figure S8. By contrast, the electrodes cycled in 20FEC:80DMC and 50FEC:50DMC still display intense C_a and C_b peaks in their C 1s spectrum. The decline of both peaks when cycling in the 2FEC:98LP30 formulation indicates decreasing FEC concentration in the electrolyte. Because FEC makes up only 2 vol % of the electrolyte, its depletion occurs much earlier than when it is used as a cosolvent. The increase in −C−O and $-CO_3$ species indicates an increase in EC and DMC decomposition. Previously observed DO components (i.e., C_a and C_b) are now most likely buried under a new layer of these carbonate products. In contrast, when cycling in the FEC cosolvent electrolytes, namely, 20FEC:80DMC and 50FEC:50DMC, the FEC reservoir is much larger. Therefore, DO species are still present in the SEI even after prolonged cycling.

Another interesting feature is the influence of the EC cosolvent on the SEI composition of Si/Gr electrodes cycled in 2FEC:98LP30. The amount of detected $-CO_3$ is the highest for this electrolyte in all analyzed states (i.e., 0.8 and 0.01 V and 1, 10, and 100 cycles). The presence of EC seems to promote the formation of more carbonate-containing SEI species, suggesting that EC decomposition occurs, even in the presence of FEC. Jung *et al.* showed that the presence of FEC reduces the decomposition of EC to a bare minimum.[20] Similarly, Jin *et al.* found that in the presence of FEC, the formation of liquid decomposition products such as LEDC is suppressed.[17] That XPS still detects EC decomposition can be explained by its high chemical sensitivity. To evaluate the effect of EC in an FEC cosolvent electrolyte, electrodes were cycled in 20FEC:40EC:40DMC, with corresponding C 1s spectra displayed in Figure S9a. The C 1s spectra after the first lithiation (0.01 V) and the first delithiation (1 cyc) show the same surface species as the spectra in Figure 4. A comparison between atomic percentages of an electrode cycled in 20FEC:80DMC (black) and 20FEC:40EC:40DMC (pink) is given in Figure S9b. The presence of EC leads to an increase of all carbon−oxygen species (i.e., −C−O, C═O/C_a, $-CO_2$, $-CO_3$, and C_b). The intensified electrolyte decomposition in the presence of EC indicates that EC decomposition products negatively affect the SEI stability, promoting stronger electrolyte decomposition. The formation of alkyl dicarbonates such as LEDC upon EC decomposition are known to be highly reactive.[48,49] Additionally, the short-chain nature of LEDC leads to a poor ability to accommodate the silicon volume changes.[17]

3.2.4. Effect of FEC on Silicon. To investigate the influence of FEC on silicon particles, Si 2p spectra are displayed in Figure 6. In general, some spectra show very noisy data, and

https://doi.org/10.1021/acsaem.2c01454
ACS Appl. Energy Mater. 2022, 5, 10710−10720

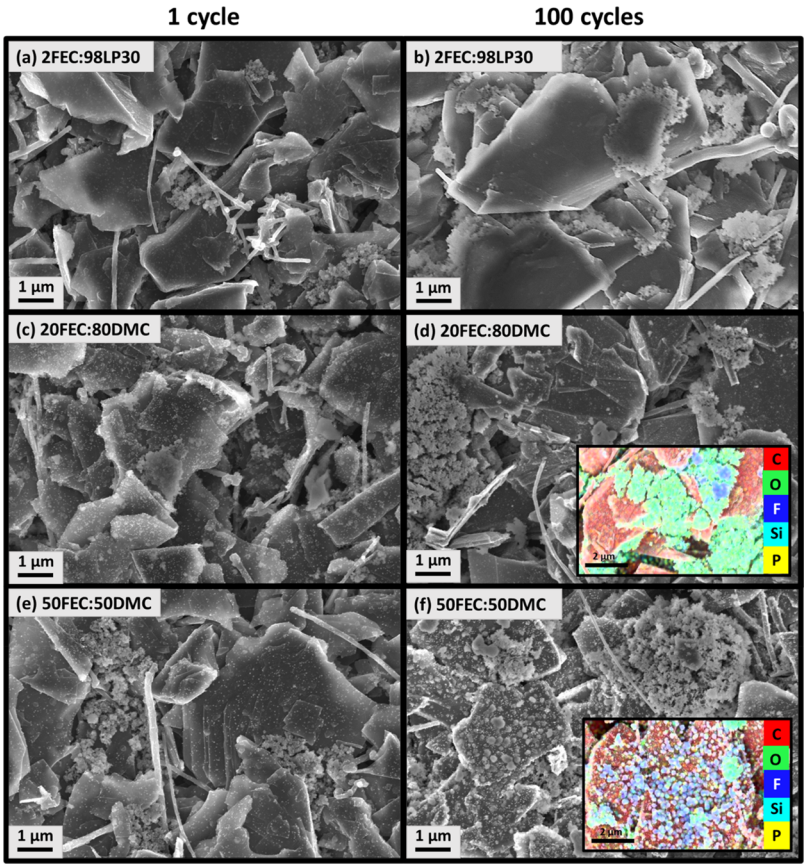

Figure 7. SEM pictures of Si/Gr electrodes cycled in (a,b) 2FEC:98LP30, (c,d) 20FEC:80DMC, and (e,f) 50FEC:50DMC after 1 and 100 cycles in the delithiated state at 1.5 V. Insets of elemental distribution for 20FEC:80DMC and 50FEC:50DMC after 100 cycles.

the peak fits are included only as a guide to the eyes. At 0.8 V, two silicon species are detected independent of the electrolyte formulation, namely, Si^0 (99 eV) and SiO_2 (~103.3 eV). These signals are also found at the surface of silicon particles in pristine Si/Gr electrodes, see Figure S10. For electrodes cycled in 20FEC:80DMC and 50FEC:50DMC electrolytes, an additional component is seen, which corresponds to SiO_xF_y (~106.3 eV). This species was also observed in the 100% FEC electrolyte previously discussed (see Figure 3). Upon lithiation to 0.01 V, the bulk silicon species, i.e., Si^0 and SiO_2, disappear in all three cases. By contrast, the SiO_xF_y species is still observed for 20FEC:80DMC and 50FEC:50DMC. After the first delithiation, the electrode cycled in the 2FEC:98LP30 electrolyte displays peaks corresponding to lithiated silicon species such as Li_xSi (98.2 eV) and Li_xSiO_y (101 eV). For this electrolyte, both species disappear after 10 cycles, but Li_xSiO_y re-emerges after 100 cycles. Electrodes cycled in 20FEC:80DMC and 50FEC:50DMC display Li_xSi and SiO_xF_y species after the first delithiation. Additionally, Li_xSiO_y is detected when using the 50FEC:50DMC electrolyte. After 10 and 100 cycles, only SiO_xF_y species are observed, and no bulk silicon re-emerges for both FEC cosolvent formulations.

As is evident from the data, the FEC concentration in the electrolyte plays a role in the silicon species detected. Two main differences are observed: (1) The re-emergence of Li_xSiO_y after 100 cycles for the 2FEC:98LP30 electrolyte is observed, while this is not the case with the two FEC cosolvent electrolytes. The re-emergence of the Li_xSiO_y species could be due to cracks in the electrode coating, resulting from the low FEC content in the electrolyte after 100 cycles. This was seen in a previous work, in which cracks in the electrode coating could be observed in cross-sectional SEM micrographs after cycling in the absence of FEC.[26] As seen in the analysis of the C 1s spectra, the SEI is predominantly made of EC and DMC decomposition products, which may lead to a less flexible SEI.[19] (2) SiO_xF_y is detected in the presence of 20FEC:80DMC and 50FEC:50DMC while not being observed at any time with 2FEC:98LP30. Interestingly, no correlation is seen between the FEC amount in the electrolyte and the amount of SiO_xF_y detected. The most extensive reporting of this compound has been done by Philippe *et al.*, who observed this species when cycling electrodes containing 80% silicon in a pure LP40 electrolyte (i.e., 1 M $LiPF_6$ in 1:1 EC:DEC), with $LiPF_6$ as the sole fluorine source.[23] The authors demonstrated this species to form during cycling as well as when storing the electrode in the electrolyte over a long period. Hard X-ray photoelectron spectroscopy (HAXPES) experiments showed SiO_xF_y to be more present in upper layers and diminishing when deeper layers were probed. These results agree with our sputtering depth profiling experiment, see Figure S11a. Interestingly, no SiO_xF_y species emerged after sputtering the electrode cycled in 2FEC:98LP30 for an extended amount of time, see Figure S11b. This is a strong indicator that this species is not formed if 9% Si/Gr anodes are cycled in the 2FEC:98LP30 electrolyte.

Furthermore, Philippe *et al.* analyzed electrodes cycled in 1 M LiFSI in 1:1 EC:DEC mixtures and could not detect any SiO_xF_y species.[24] They concluded $LiPF_6$ to play a major role in SiO_xF_y formation. To verify this hypothesis, we replaced $LiPF_6$ with LiTFSI for the 20FEC:80DMC electrolyte, and indeed,

https://doi.org/10.1021/acsaem.2c01454
ACS Appl. Energy Mater. 2022, 5, 10710−10720

no SiO_xF_y was detected, see Figure S12. As a reminder, the SEI formed by the $LiPF_6$ 20FEC:80DMC formulation displays SiO_xF_y species. This emphasized that $LiPF_6$ is crucial for the SiO_xF_y formation. To verify whether EC influences the formation of this species, we cycled electrodes in a 1 M $LiPF_6$ 20FEC:40EC:40DMC electrolyte. Despite the presence of $LiPF_6$ and FEC, no SiO_xF_y species was detected, see Figure S12. Based on all observations, the formation of SiO_xF_y is correlated with the amount of silicon in the electrode and with the presence or absence of $LiPF_6$, FEC, and EC in the electrolyte. With high silicon loadings, SiO_xF_y can still form even in the presence of EC and the absence of FEC; however, $LiPF_6$ should be the electrolyte salt. With a lower silicon loading (i.e., 9 wt %), SiO_xF_y is not detected if EC is present in the electrolyte, even if $LiPF_6$ and FEC are being used. However, in the absence of EC but the presence of FEC and $LiPF_6$, SiO_xF_y forms also at lower silicon contents. In the literature, the formation of SiO_xF_y was hypothesized to be a result of the dissolution of silica by HF, see eqs 1 and 2:[50]

$$HF + SiO_x \rightarrow SiO_xF_y + H_2O \quad (1)$$

$$H_2O + LiPF_6 \rightarrow xHF + \text{phosphates} \quad (2)$$

HF is known to form through the reaction of $LiPF_6$ with trace amounts of water. The water content in all electrolytes was determined by Karl Fischer titration to be below 10 ppm. Therefore, the amount of hydrolyzed $LiPF_6$, i.e., the amount of HF formed, should be similar for 2FEC:98LP30, 20FEC:80DMC, and 50FEC:50DMC. However, FEC can act as a source of F^- anions, which form during FEC decomposition by cleavage of the C−F bond. These F^- anions can now either react with Li^+ ions to form LiF or with silicon oxide to form SiO_xF_y compounds. However, in this case, SiO_xF_y could also be formed when cycling in 20FEC:80DMC with LiTFSI salt. This suggests that the interaction of FEC and $LiPF_6$ may play an important role in the formation of SiO_xF_y. While no experimental results can be found in the literature, molecular dynamics calculations of FEC and $LiPF_6$ exist.[51] They have shown that the presence of FEC leads to an increase in contact $Li^+-PF_6^-$ ion pairs. Contact ion pairs (CIP) are ions that are not separated by solvent molecules. This can increase the interaction between PF_6^- and Li^+ and promote the formation of PF_5, Li^+, and F^-, independent of the water content. In other words, the presence of FEC can increase the reactivity of the $LiPF_6$ salt. These CIPs may also affect the reactivity of FEC and $LiPF_6$ with respect to silicon. In the presence of EC or EC decomposition products, this reactivity might be inhibited.

In summary, using an FEC cosolvent seems to lead to a more stable SEI because no bulk Li_xSi or Li_xSiO_y species are re-emerging after cycling (which would indicate SEI dissolution or crack formation). Also, the presence of FEC and $LiPF_6$ and the absence of EC lead to the formation of SiO_xF_y at low silicon contents.

3.2.5. SEI and Electrode Morphology. SEM micrographs of electrodes cycled in the respective electrolyte for 1 and 100 cycles are presented in Figure 7. After the first cycle, all three electrodes display graphite as large rectangular shaped particles. Silicon can be seen in agglomerations of bright, small, and round particles, while carbon nanofibers emerge as long wires. Also, small bright dots are seen on graphite and nanofibers. Whether they are also present on silicon particles is difficult to assess because both emerge as bright dots in the SEM images. After 100 cycles, substantial changes in the morphology can be observed for all three cases. The surface of the electrode cycled in 2FEC:98LP30 exhibits large areas with charging effects as can be seen from the extremely bright borders on the graphite particles and silicon agglomerations. This charging can result from the accumulation of insulating SEI species. Compared to the results obtained via XPS, this could be explained by a thicker SEI layer. When cycled in the FEC cosolvent electrolytes, the electrodes show fewer charging effects and an overall better resolved morphology. This could indicate a lower accumulation of insulating SEI species and, when correlated to the XPS measurements, could be explained by a thinner SEI layer.

The small dots observed on the graphite particles already present after 1 cycle have grown to larger roundly shaped particles. This is especially the case with 50FEC:50DMC. With the help of EDS, these areas can be assigned to fluorine-containing species (blue color), see the inset in Figure 7. Elemental distribution images measured via EDS in Figure S13 further show that these particles emerge especially in the fluorine map and much less in the maps of the other elements. Similar shapes have been observed in the literature and were suggested to be LiF.[52] This assignment might also apply here because other fluorine-containing compounds such as P−F and Si−F are not seen as clearly in the respective phosphorus and silicon map, see Figure S13.

3.2.6. Correlating FEC Concentrations to SEI Properties and Electrochemical Performances. We investigated the electrochemical performance, SEI properties, and electrode morphologies of three FEC-containing electrolytes with 9% Si/Gr anodes. In this section, we bring together the different observations and findings. Similar electrochemical performances are seen for earlier cycles between 2FEC:98LP30, 20FEC:80DMC, and 50FEC:50DMC formulations. Significant differences emerge at later stages. After 100 cycles, Si/Gr anodes cycled in the 2FEC:98LP30 formulation display poor capacity retentions and a decrease in silicon and graphite activity. In contrast, the two FEC cosolvent formulations show much higher capacity retentions with higher silicon and graphite activities. SEI properties also display a dependence on the amount of FEC in the electrolyte. Compared to the FEC additive formulation, both FEC cosolvent electrolytes show a thinner SEI as determined from the XPS signal attenuation. While similar SEI compositions are observed in earlier cycling stages, differences emerge at later cycling numbers. SEM micrographs display a less charged electrode surface, and EDS shows the presence of large fluorine-containing particles, when Si/Gr anodes are cycled in both FEC cosolvent formulations.

Based on the XPS analysis, the variance in electrochemical performance can be attributed to differences in the SEI composition. The developed XPS fitting model shows FEC to decompose to −C−O-, DO-, and $-CO_2Li$-containing products. Most likely, these species are incorporated in a cross-linked polymeric network. The formation of a cross-linked polymeric network has been suggested in the literature many times.[17−19,43,44] The peaks corresponding to DO species (C_a and C_b in this work) are an unambiguous indicator for the presence of FEC decomposition products in the SEI, as this species does not form with any other electrolyte component. DO environments are detected in the SEI when cycling in 20FEC:80DMC and 50FEC:50DMC electrolytes even after 100 cycles. However, while being present in earlier cycling stages, the amount of detected DO drastically decreases after

https://doi.org/10.1021/acsaem.2c01454
ACS Appl. Energy Mater. 2022, 5, 10710−10720

longer cycling with 2FEC:98LP30. Instead, most of the observed peaks are related to −C−O and $-CO_3Li$ environments, which correspond to EC decomposition products (i.e., Li_2CO_3, LEDC, and PEO). Therefore, the good initial electrochemical performance of the electrode cycled in 2FEC:98LP30 is explained by the presence FEC decomposition products in the SEI. The formed polymeric network increases the ability of the SEI to better accommodate the silicon volume changes. However, this network might not form a perfectly elastic SEI as it still cracks and leads to recurrent FEC reduction. In the case of 2FEC:98LP30, the continuous consumption of FEC eventually depletes the electrolyte of the additive. Simultaneously, an increase in EC reduction occurs, which ultimately leads to an SEI that is composed of short-chain LEDC and PEO components. These components are less fit to accommodate the silicon volume changes.[43] Hence, the SEI fractures and the electrode material is re-exposed (see the Li_xSiO_y peak for the 2FEC:98LP30 case). Consequently, a new SEI is formed on the re-exposed surfaces. This excessive SEI formation can ultimately lead to the isolation of silicon particles and reduced electrode integrity. The loss in graphite and silicon activity observed for the 2FEC:98LP30 electrolyte formulation could be explained by this phenomenon. In contrast, when cycling in 20FEC:80DMC and 50FEC:50DMC, FEC decomposition products (indicated by DO environments) are present in the SEI for a longer period because the FEC reservoir in the electrolyte is larger. Also, since EC is not present in the electrolyte, its decomposition products are absent in the SEI. Consequently, the SEI is more stable, and less electrolyte is decomposed. The extended presence of the polymeric network buffers the silicon volume changes, reduces the amount of the SEI formed, and helps to maintain the electrode integrity for a longer time. This would explain the smaller decrease in silicon and graphite activity when cycling in the FEC cosolvent electrolytes. The presence of this polymer in the SEI seems therefore crucial for a good electrochemical performance.

A further interesting observation is the emergence of SiO_xF_y species, which are detected when using the FEC cosolvent formulations but not the FEC additive electrolyte. Translating the findings from Philippe *et al.* with pure silicon to Si/Gr anodes, SiO_xF_y may decrease the affinity between the binder and the surface of the active material.[24] This would result in a poor electrochemical performance. However, the proposed negative impact of SiO_xF_y does not seem to be that detrimental to the performance because cells cycled in 20FEC:80DMC and 50FEC:50DMC electrolytes show superior capacity retention. Therefore, the suggested negative effect of SiO_xF_y most probably has an inferior impact on the SEI stability. Instead, the volume accommodating effect of the polymeric network seems to have a much higher influence on the electrochemical performance of Si/Gr electrodes.

In summary, FEC cosolvent electrolytes offer two advantages: (1) the positive effect of a polymeric network containing −C−O, DO, and $-CO_2$ species is preserved for much longer, and (2) no EC decomposition products are present in the SEI, which leads to a more stable surface layer and lower overall electrolyte consumption.

4. CONCLUSIONS

Our study examined how using FEC as a cosolvent influenced the electrochemical performance, SEI thickness, and composition, as well as the electrode morphology of Si/Gr composite electrodes. Two electrolyte formulations (20FEC:80DMC and 50FEC:50DMC) were compared to a reference electrolyte with FEC as an electrolyte additive (2FEC:98LP30). The developed XPS fitting model showed FEC to decompose to −C−O-, DO-, and $-CO_2Li$-containing products. Most likely, these species were incorporated in a cross-linked polymeric network. The two chemical environments in DO (C_a and C_b) enabled us to unambiguously trace the presence of FEC decomposition products in the SEI. Compared to the additive concentration, both FEC cosolvent mixtures showed the following:

(1) a thinner SEI as determined from XPS
(2) a high amount of FEC decomposition products (as indicated by C_a and C_b) present in the SEI even after longer cycling, while these species strongly decreased for the FEC additive electrolyte
(3) reduced decomposition of DMC cosolvents (and the absence of EC decomposition products)
(4) a lower amount of carbonate species
(5) formation of SiO_xF_y species, suggesting the presence of FEC and the absence of EC to promote the formation of this species

The improved electrochemical performance of the FEC cosolvent formulations originates from the presence of FEC decomposition products in the SEI even after 100 cycles, consisting of a polymeric network containing −C−O, DO, and $-CO_2Li$ units. The presence of this polymeric network species is crucial in stabilizing the SEI upon the silicon volume changes. Most probably, it increases the flexibility of the surface layer, which reduces the number of cracks in the SEI. In this way, less active material is re-exposed to the electrolyte, reducing the amount of the new SEI formed and thereby extending the lifetime of the cell. The prolonged presence of this polymeric species is especially essential when moving toward applications with higher silicon contents.

■ ASSOCIATED CONTENT

Supporting Information

The Supporting Information is available free of charge at https://pubs.acs.org/doi/10.1021/acsaem.2c01454.

Additional information on electrochemical dQ/dE data; XPS data containing information about SEI thickness, additional spectra, and atomic percentage tables (PDF)

■ AUTHOR INFORMATION

Corresponding Author

Julia Maibach − *Karlsruhe Institute of Technology (KIT), Institute for Applied Materials−Energy Storage Systems (IAM-ESS), Eggenstein-Leopoldshafen 76344, Germany;* orcid.org/0000-0003-1339-7804; Email: julia.maibach@kit.edu

Authors

Lydia Gehrlein − *Karlsruhe Institute of Technology (KIT), Institute for Applied Materials−Energy Storage Systems (IAM-ESS), Eggenstein-Leopoldshafen 76344, Germany;* orcid.org/0000-0003-4739-8928

Christian Njel − *Karlsruhe Institute of Technology (KIT), Institute for Applied Materials−Energy Storage Systems (IAM-ESS), Eggenstein-Leopoldshafen 76344, Germany*

Fabian Jeschull − *Karlsruhe Institute of Technology (KIT), Institute for Applied Materials−Energy Storage Systems*

https://doi.org/10.1021/acsaem.2c01454
ACS Appl. Energy Mater. 2022, 5, 10710−10720

(IAM-ESS), Eggenstein-Leopoldshafen 76344, Germany; orcid.org/0000-0002-5927-1978

Complete contact information is available at: https://pubs.acs.org/10.1021/acsaem.2c01454

Notes

The authors declare no competing financial interest.

■ ACKNOWLEDGMENTS

The authors are grateful to the German Federal Ministry of Education and Research (FKZ 03XP0131) for financial support. The authors would also like to thank Tim Bastek and Celine Roeder for their preliminary work on this topic. This work contributes to the research performed at CELEST (Center for Electrochemical Energy Storage Ulm-Karlsruhe).

■ REFERENCES

(1) Goodenough, J. B.; Kim, Y. Challenges for Rechargeable Li Batteries †. *Chem. Mater.* **2010**, *22*, 587−603.
(2) Chung, G.-C.; Kim, H.-J.; Yu, S.-I.; Jun, S.-H.; Choi, J.; Kim, M.-H. Origin of Graphite Exfoliation An Investigation of the Important Role of Solvent Cointercalation. *J. Electrochem. Soc.* **2000**, *147*, 4391.
(3) Obrovac, M. N.; Krause, L. J. Reversible Cycling of Crystalline Silicon Powder. *J. Electrochem. Soc.* **2007**, *154*, A103.
(4) Obrovac, M. N.; Christensen, L.; Le, D. B.; Dahn, J. R. Alloy Design for Lithium-Ion Battery Anodes. *J. Electrochem. Soc.* **2007**, *154*, A849.
(5) Obrovac, M. N.; Chevrier, V. L. Alloy Negative Electrodes for Li-Ion Batteries. *Chem. Rev.* **2014**, *114*, 11444−11502.
(6) Iaboni, D. S. M.; Obrovac, M. N. Li 15 Si 4 Formation in Silicon Thin Film Negative Electrodes. *J. Electrochem. Soc.* **2016**, *163*, A255−A261.
(7) Wetjen, M.; Pritzl, D.; Jung, R.; Solchenbach, S.; Ghadimi, R.; Gasteiger, H. A. Differentiating the Degradation Phenomena in Silicon-Graphite Electrodes for Lithium-Ion Batteries. *J. Electrochem. Soc.* **2017**, *164*, A2840−A2852.
(8) Chae, S.; Choi, S. H.; Kim, N.; Sung, J.; Cho, J. Integration of Graphite and Silicon Anodes for the Commercialization of High-Energy Lithium-Ion Batteries. *Angew. Chem., Int. Ed.* **2020**, *59*, 110−135.
(9) Jeschull, F.; Surace, Y.; Zürcher, S.; Spahr, M. E.; Novák, P.; Trabesinger, S. Electrochemistry and Morphology of Graphite Negative Electrodes Containing Silicon as Capacity-Enhancing Electrode Additive. *Electrochim. Acta* **2019**, *320*, 1−12.
(10) Karkar, Z.; Mazouzi, D.; Hernandez, C. R.; Guyomard, D.; Roué, L.; Lestriez, B. Threshold-like Dependence of Silicon-Based Electrode Performance on Active Mass Loading and Nature of Carbon Conductive Additive. *Electrochim. Acta* **2016**, *215*, 276−288.
(11) Chen, H.; Wang, Z.; Hou, X.; Fu, L.; Wang, S.; Hu, X.; Qin, H.; Wu, Y.; Ru, Q.; Liu, X.; Hu, S. Mass-Producible Method for Preparation of a Carbon-Coated Graphite@plasma Nano-Silicon@carbon Composite with Enhanced Performance as Lithium Ion Battery Anode. *Electrochim. Acta* **2017**, *249*, 113−121.
(12) Mazouzi, D.; Karkar, Z.; Hernandez, C. R.; Manero, P. J.; Guyomard, D.; Roué, L.; Lestriez, B. Critical Roles of Binders and Formulation at Multiscales of Silicon-Based Composite Electrodes. *J. Power Sources* **2015**, *280*, 533−549.
(13) Lestriez, B.; Desaever, S.; Danet, J.; Moreau, P.; Plée, D.; Guyomard, D. Hierarchical and Resilient Conductive Network of Bridged Carbon Nanotubes and Nanofibers for High-Energy Si Negative Electrodes. *Electrochem. Solid-State Lett.* **2009**, *12*, A76−A80.
(14) Schott, T.; Robert, R.; Ulmann, P. A.; Lanz, P.; Zürcher, S.; Spahr, M. E.; Novák, P.; Trabesinger, S. Cycling Behavior of Silicon-Containing Graphite Electrodes, Part A: Effect of the Lithiation Protocol. *J. Phys. Chem. C* **2017**, *121*, 18423−18429.
(15) Verma, P.; Maire, P.; Novák, P. A Review of the Features and Analyses of the Solid Electrolyte Interphase in Li-Ion Batteries. *Electrochim. Acta* **2010**, *55*, 6332−6341.
(16) Heiskanen, S. K.; Kim, J.; Lucht, B. L. Generation and Evolution of the Solid Electrolyte Interphase of Lithium-Ion Batteries. *Joule* **2019**, *3*, 2322−2333.
(17) Jin, Y.; Kneusels, N. J. H.; Magusin, P. C. M. M.; Kim, G.; Castillo-Martínez, E.; Marbella, L. E.; Kerber, R. N.; Howe, D. J.; Paul, S.; Liu, T.; Grey, C. P. Identifying the Structural Basis for the Increased Stability of the Solid Electrolyte Interphase Formed on Silicon with the Additive Fluoroethylene Carbonate. *J. Am. Chem. Soc.* **2017**, *139*, 14992−15004.
(18) Michan, A. L.; Parimalam, B. S.; Leskes, M.; Kerber, R. N.; Yoon, T.; Grey, C. P.; Lucht, B. L. Fluoroethylene Carbonate and Vinylene Carbonate Reduction: Understanding Lithium-Ion Battery Electrolyte Additives and Solid Electrolyte Interphase Formation. *Chem. Mater.* **2016**, *28*, 8149−8159.
(19) Jin, Y.; Kneusels, N. J. H.; Marbella, L. E.; Castillo-Martínez, E.; Magusin, P. C. M. M.; Weatherup, R. S.; Jónsson, E.; Liu, T.; Paul, S.; Grey, C. P. Understanding Fluoroethylene Carbonate and Vinylene Carbonate Based Electrolytes for Si Anodes in Lithium Ion Batteries with NMR Spectroscopy. *J. Am. Chem. Soc.* **2018**, *140*, 9854−9867.
(20) Jung, R.; Metzger, M.; Haering, D.; Solchenbach, S.; Marino, C.; Tsiouvaras, N.; Stinner, C.; Gasteiger, H. A. Consumption of Fluoroethylene Carbonate (FEC) on Si-C Composite Electrodes for Li-Ion Batteries. *J. Electrochem. Soc.* **2016**, *163*, A1705−A1716.
(21) Schiele, A.; Breitung, B.; Hatsukade, T.; Berkes, B. B.; Hartmann, P.; Janek, J.; Brezesinski, T. The Critical Role of Fluoroethylene Carbonate in the Gassing of Silicon Anodes for Lithium-Ion Batteries. *ACS Energy Lett.* **2017**, *2*, 2228−2233.
(22) Xu, C.; Lindgren, F.; Philippe, B.; Gorgoi, M.; Björefors, F.; Edström, K.; Gustafsson, T. Improved Performance of the Silicon Anode for Li-Ion Batteries: Understanding the Surface Modification Mechanism of Fluoroethylene Carbonate as an Effective Electrolyte Additive. *Chem. Mater.* **2015**, *27*, 2591−2599.
(23) Philippe, B.; Dedryveère, R.; Gorgoi, M.; Rensmo, H.; Gonbeau, D.; Edström, K. Role of the LiPF6 Salt for the Long-Term Stability of Silicon Electrodes in Li-Ion Batteries - A Photoelectron Spectroscopy Study. *Chem. Mater.* **2013**, *25*, 394−404.
(24) Philippe, B.; Dedryveère, R.; Gorgoi, M.; Rensmo, H.; Gonbeau, D.; Edström, K. Improved Performances of Nanosilicon Electrodes Using the Salt LiFSI: A Photoelectron Spectroscopy Study. *J. Am. Chem. Soc.* **2013**, *135*, 9829−9842.
(25) Markevich, E.; Salitra, G.; Aurbach, D. Fluoroethylene Carbonate as an Important Component for the Formation of an Effective Solid Electrolyte Interphase on Anodes and Cathodes for Advanced Li-Ion Batteries. *ACS Energy Lett.* **2017**, *2*, 1337−1345.
(26) Ghamlouche, A.; Müller, M.; Jeschull, F.; Maibach, J. Degradation Phenomena in Silicon/Graphite Electrodes with Varying Silicon Content. *J. Electrochem. Soc.* **2022**, *169*, No. 020541.
(27) Breitung, B.; Schneider, A.; Chakravadhanula, V. S. K.; Suchomski, C.; Janek, J.; Sommer, H.; Brezesinski, T. Artificial Composite Anode Comprising High-Capacity Silicon and Carbonaceous Nanostructures for Long Cycle Life Lithium-Ion Batteries. *Battery Supercaps* **2018**, *1*, 27−32.
(28) Breitung, B.; Baumann, P.; Sommer, H.; Janek, J.; Brezesinski, T. In Situ and Operando Atomic Force Microscopy of High-Capacity Nano-Silicon Based Electrodes for Lithium-Ion Batteries. *Nanoscale* **2016**, *8*, 14048−14056.
(29) Lavi, O.; Luski, S.; Shpigel, N.; Menachem, C.; Pomerantz, Z.; Elias, Y.; Aurbach, D. Electrolyte Solutions for Rechargeable Li-Ion Batteries Based on Fluorinated Solvents. *ACS Appl. Energy Mater.* **2020**, *3*, 7485−7499.
(30) Markevich, E.; Salitra, G.; Fridman, K.; Sharabi, R.; Gershinsky, G.; Garsuch, A.; Semrau, G.; Schmidt, M. A.; Aurbach, D. Fluoroethylene Carbonate as an Important Component in Electrolyte Solutions for High-Voltage Lithium Batteries: Role of Surface Chemistry on the Cathode. *Langmuir* **2014**, *30*, 7414−7424.

(31) Salitra, G.; Markevich, E.; Afri, M.; Talyosef, Y.; Hartmann, P.; Kulisch, J.; Sun, Y. K.; Aurbach, D. High-Performance Cells Containing Lithium Metal Anodes, LiNi0. 6Co0.2Mn0.2O2 (NCM 622) Cathodes, and Fluoroethylene Carbonate-Based Electrolyte Solution with Practical Loading. *ACS Appl. Mater. Interfaces* **2018**, *10*, 19773−19782.
(32) Parry, K. L.; Shard, A. G.; Short, R. D.; White, R. G.; Whittle, J. D.; Wright, A. ARXPS Characterisation of Plasma Polymerised Surface Chemical Gradients. *Surf. Interface Anal.* **2006**, *38*, 1497−1504.
(33) Etacheri, V.; Haik, O.; Goffer, Y.; Roberts, G. A.; Stefan, I. C.; Fasching, R.; Aurbach, D. Effect of Fluoroethylene Carbonate (FEC) on the Performance and Surface Chemistry of Si-Nanowire Li-Ion Battery Anodes. *Langmuir* **2012**, *28*, 965−976.
(34) Petibon, R.; Chevrier, V. L.; Aiken, C. P.; Hall, D. S.; Hyatt, S. R.; Shunmugasundaram, R.; Dahn, J. R. Studies of the Capacity Fade Mechanisms of LiCoO 2 /Si-Alloy: Graphite Cells. *J. Electrochem. Soc.* **2016**, *163*, A1146−A1156.
(35) Jaumann, T.; Balach, J.; Langklotz, U.; Sauchuk, V.; Fritsch, M.; Michaelis, A.; Teltevskij, V.; Mikhailova, D.; Oswald, S.; Klose, M.; Stephani, G.; Hauser, R.; Eckert, J.; Giebeler, L. Lifetime vs. Rate Capability: Understanding the Role of FEC and VC in High-Energy Li-Ion Batteries with Nano-Silicon Anodes. *Energy Storage Mater.* **2017**, *6*, 26−35.
(36) Jaumann, T.; Balach, J.; Klose, M.; Oswald, S.; Langklotz, U.; Michaelis, A.; Eckert, J.; Giebeler, L. SEI-Component Formation on Sub 5 Nm Sized Silicon Nanoparticles in Li-Ion Batteries: The Role of Electrode Preparation, FEC Addition and Binders. *Phys. Chem. Chem. Phys.* **2015**, *17*, 24956−24967.
(37) Schroder, K.; Alvarado, J.; Yersak, T. A.; Li, J.; Dudney, N.; Webb, L. J.; Meng, Y. S.; Stevenson, K. J. The Effect of Fluoroethylene Carbonate as an Additive on the Solid Electrolyte Interphase on Silicon Lithium-Ion Electrodes. *Chem. Mater.* **2015**, *27*, 5531−5542.
(38) Chen, X.; Li, X.; Mei, D.; Feng, J.; Hu, M. Y.; Hu, J.; Engelhard, M.; Zheng, J.; Xu, W.; Xiao, J.; Liu, J.; Zhang, J. G. Reduction Mechanism of Fluoroethylene Carbonate for Stable Solid-Electrolyte Interphase Film on Silicon Anode. *ChemSusChem* **2014**, *7*, 549−554.
(39) An, S. J.; Li, J.; Daniel, C.; Mohanty, D.; Nagpure, S.; Wood, D. L., III The State of Understanding of the Lithium-Ion-Battery Graphite Solid Electrolyte Interphase (SEI) and Its Relationship to Formation Cycling. *Carbon N. Y.* **2016**, *105*, 52−76.
(40) Cao, C.; Steinrück, H. G.; Shyam, B.; Toney, M. F. The Atomic Scale Electrochemical Lithiation and Delithiation Process of Silicon. *Adv. Mater. Interfaces* **2017**, *4*, 1−7.
(41) Fears, T. M.; Doucet, M.; Browning, J. F.; Baldwin, J. K. S.; Winiarz, J. G.; Kaiser, H.; Taub, H.; Sacci, R. L.; Veith, G. M. Evaluating the Solid Electrolyte Interphase Formed on Silicon Electrodes: A Comparison of: Ex Situ X-Ray Photoelectron Spectroscopy and in Situ Neutron Reflectometry. *Phys. Chem. Chem. Phys.* **2016**, *18*, 13927−13940.
(42) El Ouatani, L.; Dedryvère, R.; Siret, C.; Biensan, P.; Reynaud, S.; Iratçabal, P.; Gonbeau, D. The Effect of Vinylene Carbonate Additive on Surface Film Formation on Both Electrodes in Li-Ion Batteries. *J. Electrochem. Soc.* **2009**, *156*, A103.
(43) Kamikawa, Y.; Amezawa, K.; Terada, K. First-Principles Study on the Mechanical Properties of Polymers Formed by the Electrochemical Reduction of Fluoroethylene Carbonate and Vinylene Carbonate. *J. Phys. Chem. C* **2020**, *124*, 19937−19944.
(44) Shkrob, I. A.; Wishart, J. F.; Abraham, D. P. What Makes Fluoroethylene Carbonate Different? *J. Phys. Chem. C* **2015**, *119*, 14954−14964.
(45) Bosman, H. J. M.; Pijpers, A. P.; Jaspers, A. W. M. A. An X-Ray Photoelectron Spectroscopy Study of the Acidity of SiO2-ZrO2 Mixed Oxides. *J. Catal.* **1996**, *161*, 551−559.
(46) Maibach, J.; Lindgren, F.; Eriksson, H.; Edström, K.; Hahlin, M. Electric Potential Gradient at the Buried Interface between Lithium-Ion Battery Electrodes and the SEI Observed Using Photoelectron Spectroscopy. *J. Phys. Chem. Lett.* **2016**, *7*, 40.
(47) Lindgren, F.; Rehnlund, D.; Källquist, I.; Nyholm, L.; Edström, K.; Hahlin, M.; Maibach, J. Breaking Down a Complex System: Interpreting PES Peak Positions for Cycled Li-Ion Battery Electrodes. *J. Phys. Chem. C* **2017**, *121*, 27303−27312.
(48) Yoon, T.; Milien, M. S.; Parimalam, B. S.; Lucht, B. L. Thermal Decomposition of the Solid Electrolyte Interphase (SEI) on Silicon Electrodes for Lithium Ion Batteries. *Chem. Mater.* **2017**, *29*, 3237−3245.
(49) Parimalam, B. S.; MacIntosh, A. D.; Kadam, R.; Lucht, B. L. Decomposition Reactions of Anode Solid Electrolyte Interphase (SEI) Components with LiPF6. *J. Phys. Chem. C* **2017**, *121*, 22733−22738.
(50) Ha, Y.; Stetson, C.; Harvey, S. P.; Teeter, G.; Tremolet De Villers, B. J.; Jiang, C. S.; Schnabel, M.; Stradins, P.; Burrell, A.; Han, S. D. Effect of Water Concentration in LiPF6-Based Electrolytes on the Formation, Evolution, and Properties of the Solid Electrolyte Interphase on Si Anodes. *ACS Appl. Mater. Interfaces* **2020**, *12*, 49563−49573.
(51) Hou, T.; Yang, G.; Rajput, N. N.; Self, J.; Park, S. W.; Nanda, J.; Persson, K. A. The Influence of FEC on the Solvation Structure and Reduction Reaction of LiPF6/EC Electrolytes and Its Implication for Solid Electrolyte Interphase Formation. *Nano Energy* **2019**, *64*, 103881.
(52) Surace, Y.; Leanza, D.; Mirolo, M.; Kondracki, L.; Vaz, C. A. F.; El Kazzi, M.; Novák, P.; Trabesinger, S. Evidence for Stepwise Formation of Solid Electrolyte Interphase in a Li-Ion Battery. *Energy Storage Mater.* **2021**, *44*, 156−167.

https://doi.org/10.1021/acsaem.2c01454
ACS Appl. Energy Mater. 2022, 5, 10710−10720